High-pressure elasticity of alumina studied by first principles

WENHUI DUAN, BIJAYA B. KARKI, AND RENATA M. WENTZCOVITCH*

Department of Chemical Engineering and Materials Science, and Minnesota Supercomputing Institute, University of Minnesota, Minneapolis, Minnesota 55455, U.S.A.

ABSTRACT

We investigate by first principles the elastic behavior of Al_2O_3-alumina under pressure (up to 300 GPa) in the corundum and Rh_2O_3 (II) phase. The results are in excellent agreement with available low pressure (<1 GPa) experimental data. The anisotropy in elasticity for corundum decreases up to 50 GPa and then increases slowly with pressure whereas for the Rh_2O_3 (II) phase the anisotropy increases monotonically with compression. Strong shear wave anisotropy in the Rh_2O_3 (II) phase is found to be associated with the relatively small c_{55} modulus, and its softening at high pressures. Unlike corundum, the directions of the fastest and slowest wave propagation, and the maximum polarization anisotropy of Rh_2O_3 (II) phase remain unchanged with pressure. At the corundum to Rh_2O_3 (II) phase transition pressure (78 GPa at 0 K), the anisotropy increases by more than 100% but the density and wave velocities increase only by 2%. The calculated (0 K) densities and wave velocities at lower mantle pressures are slightly larger (by 5%) than the corresponding seismic profiles. Our results suggest that the presence of free Al_2O_3 in small amounts in the lower mantle may not be detected in seismic density and velocity profile. However, its anisotropy may produce a detectable signal, particularly, at pressure conditions typical of the D" region.

INTRODUCTION

Al_2O_3 (alumina) is of great interest due to its diverse applications in high-pressure science. The pressure-dependence of the R fluorescence lines of Cr^{+3}-doped Al_2O_3-corundum (ruby) provides a convenient and accurate technique for pressure calibration in diamond-anvil cell experiments. It is also used as a window material in dynamic shock-wave measurements and is a useful ceramic material. Finally, free Al_2O_3 may exist in the lower mantle in small amounts, making up about 3.6% (in mass) of the mineralogical composition of this region (Anderson 1989; Brown and Mussett 1993).

Recent X-ray diffraction experiment observed that ruby undergoes a transformation to the Rh_2O_3 (II) structure when heated to 1000 K and pressurized to ~100 GPa (Funamori and Jeanloz 1997). At room temperature, experiments have shown a wide stability field of corundum up to pressure of 180 GPa (Richet et al. 1988; Jephcoat et al. 1988). However, several theoretical investigations have suggested the possibility of structural transformation of corundum to Rh_2O_3 (II) phase at much lower pressure at zero temperature (Cynn et al. 1990; Marton and Cohen 1994; Thomson et al. 1996; Duan et al. 1998). The latest study of six alumina polymorphs (Duan et al. 1998), namely, corundum, Rh_2O_3 (II), *Pbnm* perovskite, $R\bar{3}c$-perovskite, A-type rare-earth sesquioxide and B-type rare-earth sesquioxide, confirmed previous prediction of two phase transitions: corundum →

Rh_2O_3 (II) at 78 ± 4 GPa and Rh_2O_3 (II) → *Pbnm* perovskite at 223 ± 10 GPa. The first one is in good agreement with the all electron linearized augmented plane wave (LAPW) value of 90 GPa (Marton and Cohen 1994).

Measurements of individual elastic constants of Al_2O_3 exist up to 1 GPa (Gieske and Barsch 1968) whereas their temperature dependencies have been measured up to 1825 K (Goto et al. 1989). The pressure dependence of isotropic wave velocities have been studied up to 61.6 GPa by Zhang and Chopelas (1994) from side-band fluorescence measurements. Cohen (1987) has studied the pressure dependence of elastic constants of corundum using the potential-induced breathing (PIB) model. Because the PIB model makes some crucial approximations to the nature of bonding such as full ionization, spherical ions, and use of pairwise interactions, the high pressure elasticity should ultimately be reinvestigated by a first-principles method. This paper reports the elastic constants (c_{ij}) of two alumina polymorphs, corundum and Rh_2O_3 (II), as a function of pressure up to 300 GPa. Using the calculated elastic constants, we study the pressure dependence of the elastic anisotropy and wave velocities of the mineral and speculate on the geophysical implications of these results.

CALCULATED ELASTIC CONSTANTS

Full structural optimization is performed using first principles variable cell shape molecular dynamics (Wentzcovitch et al. 1993) within the local density approximation (LDA). Norm-conserving Troullier and Martins (1991) pseudopotentials are used with plane-wave energy cut-offs of 70 Ry for electronic wavefunctions. Brillouin Zone sampling is performed using spe-

---

*E-mail: wentzcov@cems.umn.edu

cial points in the irreducible wedge ($2 \times 2 \times 2$ regular grid). For computational details see Thomson et al. (1996) and Duan et al. (1998). The Full elastic constant tensor is determined from the stresses generated by small deformations of the optimized cell at a given pressure (e.g., Wentzcovitch et al. 1995; Karki et al. 1997; Wentzcovitch et al. 1998).

The corundum to Rh_2O_3 (II) structural transformation is predicted to take place at 78 ± 4 GPa (Thomson et al. 1996). These structures are very similar and can be viewed as made up of edge-sharing AlO_6 octahedra (Shannon and Prewitt 1978). In corundum, the octahedra share three edges while in Rh_2O_3 (II) they share two. Here we determine the elastic constants of these alumina phases as a function of pressure. Corundum having trigonal symmetry (space group $R\bar{3}c$) is characterized by six independent elastic coefficients c_{11}, c_{33}, c_{44}, c_{12}, c_{13}, and c_{14}, whereas the orthorhombic Rh_2O_3 (II) phase (space group $Pbna$) by nine constants, c_{11}, c_{22}, c_{33}, c_{44}, c_{55}, c_{66}, c_{12}, c_{13}, and c_{23} (Musgrave 1970). The calculated constants and their pressure derivatives at zero pressure for corundum (Table 1) compare favorably with ambient condition experimental data (Gieske and Barsch 1968) and our results represent an improvement over the previous calculations based on PIB model (Cohen 1987). The temperature difference of 300 K (because our computations are athermal) and the overbinding effects of the local density approximation used in this method tend to make the elastic constants slightly larger than the measured values.

Pressure variations of the elastic constants are shown in Figure 1. For corundum, two longitudinal elastic constants (c_{11} and c_{33}) are almost equal at zero pressure but they slightly depart from each other (c_{11} being larger than c_{33}) at high pressures, indicating that the c axis is more compressible than the a axis, consistent with our structural analysis (Duan et al. 1998) and with experiments (Finger and Hazen 1978). With increasing pressure, c_{14} increases to zero and changes sign at about 90

GPa. For the Rh_2O_3 (II) phase, the elastic constant c_{33} remains much larger than c_{11} and c_{22} throughout the pressure regime studied, indicating clearly that the c axis is the least compressible. With increasing pressure, c_{11} becomes increasingly larger than c_{22} so the b axis becomes the most compressible at high pressures (Duan et al. 1998). The shear elastic constants (c_{44}, c_{55}, c_{66}) increasingly diverge under compression, and one of them, c_{55}, increases slowly at first and then starts to soften above 150 GPa.

The isotropic bulk (K) and shear (G) moduli (Table 1) are determined using the Voigt-Ruess-Hill averaging scheme (Hill 1952). The upper (Voigt) and lower (Ruess) bounds in the bulk modulus are much closer than those in the shear modulus. For corundum, the difference between upper and lower bounds in the shear modulus increases from 3 GPa at zero pressure to 6 GPa at $P = 150$ GPa whereas that for Rh_2O_3 (II) phase increases from 8 GPa at $P = 75$ GPa to 66 GPa at $P = 300$ GPa.

TABLE 1. Zero pressure elastic constants (in GPa) and their pressure derivatives of corundum (from third-order finite strain equations) compared with previous studies

	c_{11}	c_{33}	c_{44}	c_{12}	c_{13}	c_{14}	K	G
Calculated (this work)								
M	502	501	157	161	125	−19	258	168
$\partial M/\partial P$	5.52	5.10	2.03	3.09	3.57	0.19	4.06	1.44
Experimental (Gieske and Barsch 1968)								
M	498	502	147	163	117	−23	255	163
$\partial M/\partial P$	6.17	5.00	2.24	3.28	3.65	0.13	4.30	1.64
PIB model (Cohen 1987)								
M	540	455	157	157	130	−48	262	169
$\partial M/\partial P$	5.78	4.36	1.62	3.44	3.56	0.18	4.09	1.37
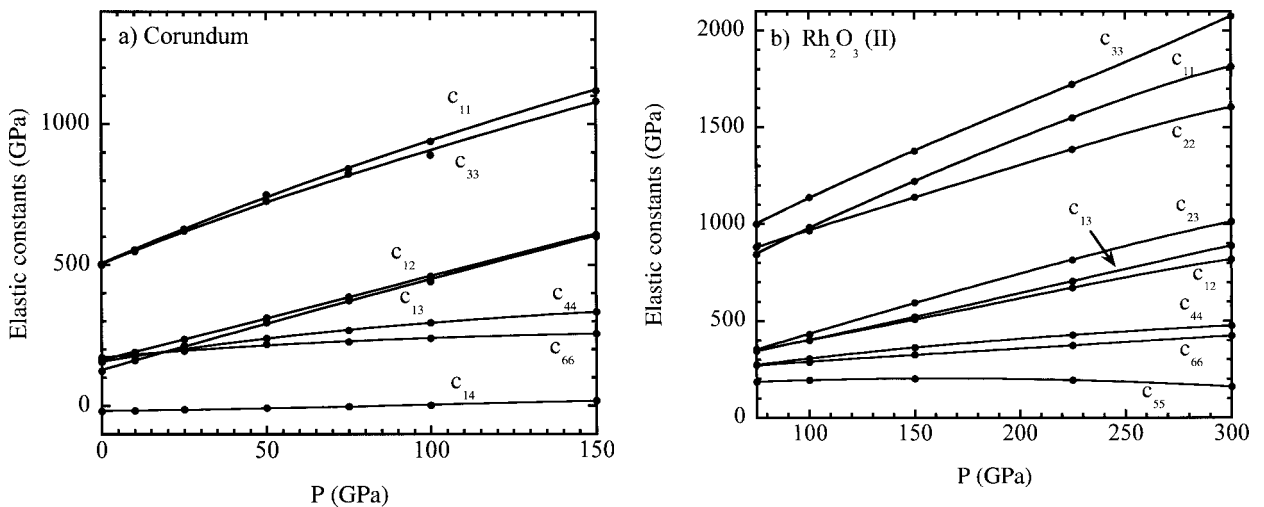
FIGURE 1. Pressure dependence of the elastic moduli (c_{ij}) of (**a**) corundum and (**b**) Rh_2O_3 (II) phase of Al_2O_3.

SINGLE-CRYSTAL WAVE VELOCITIES AND ANISOTROPY

We determine the single crystal elastic wave velocities as a function of propagation direction by solving Christoffel's equation (Musgrave 1970)

$$\det(c_{ijkl}\mathbf{n}_j\mathbf{n}_l - \rho V^2\delta_{ik}) = 0 \qquad (1)$$

where c_{ijkl} is the single crystal elastic constant tensor, $\mathbf{n}$ is the propagation direction, ρ is the density, and δ_{ij} is the Kronecker delta function. The eigenvalues of the 3×3 matrix yield the three unique elastic wave velocities [one compressional (V_P) and two shear (V_S) waves] for a given propagation direction while the eigenvectors give the polarization directions. We express the azimuthal anisotropy for P- and S-waves as follows:

$$A = \frac{V_{\max} - V_{\min}}{<V>} \times 100 \qquad (2)$$

where

$$\langle V \rangle = \sqrt{\frac{K + \frac{4}{3}G}{\rho}} \text{ for P-wave; } \langle V \rangle = \sqrt{\frac{G}{\rho}} \text{ for S-wave} \qquad (3)$$

are the isotropic aggregate velocities. Because two shear waves exist for a given propagation direction, we can also define the S-wave polarization anisotropy.

Figure 2 shows the angular variations of the velocities for corundum at zero pressure. The velocities in the xy plane depend slightly on the direction. This weak anisotropy solely comes from
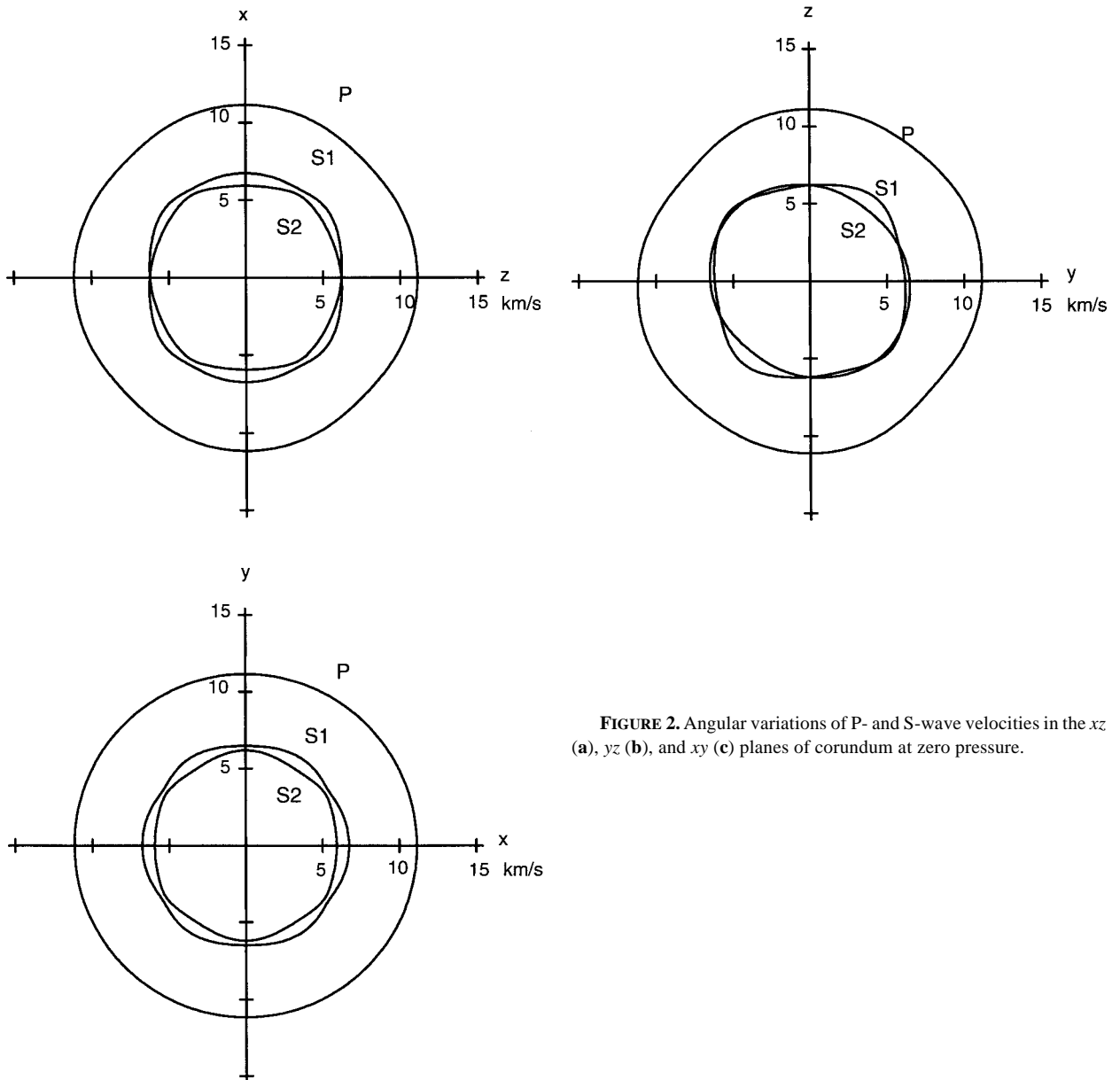
FIGURE 2. Angular variations of P- and S-wave velocities in the xz (**a**), yz (**b**), and xy (**c**) planes of corundum at zero pressure.

the small value of c_{14}. Both yz and zx planes show stronger anisotropy than does the basal (xy) plane. If c_{14} is zero, system becomes transversely isotropic as in the case of a hexagonal symmetry (Musgrave 1970). The value of c_{14} is zero at pressure of about 90 GPa so corundum becomes transversely isotropic at this pressure. Pressure variation of the overall azimuthal and polarization anisotropy factors are shown in Figure 3. The S-wave anisotropy is much stronger than the P-wave anisotropy (16% azimuthal and polarization variations for S-wave, and 7% azimuthal variation for P-wave at zero pressure). As pressure rises, the anisotropy of corundum strongly decreases up to 50 GPa, and then slowly increases at higher pressures. At zero pressure, the fastest and slowest P-wave propagation directions are close to $[01^{1}/_{4}]$ and $[011]$ respectively, whereas both fastest and slowest S-waves are contained in the direction close to $[011]$, as shown in Figure 2. These directions change with pressure in a complicated manner. The maximum polarization anisotropy of S-waves which occurs in the direction close to $[011]$ at 0 and 10 GPa changes to the direction $[100]$ at higher pressures due to smaller value of c_{66} than c_{44}.

Anisotropies increase by more than a factor of two at the corundum to Rh_2O_3 (II) phase transition in alumina (Fig. 3). At 100 GPa, P-waves show 11% azimuthal anisotropy whereas S-waves show 25% azimuthal and 21% polarization anisotropy. The P-wave anisotropy of Rh_2O_3 (II) phase shows a slight increase with pressure (Fig. 3). However, the S-wave anisotropy

strongly increases with pressure (Fig. 3) because c_{55} increases slowly and eventually softens under compression (Fig. 1). The slowest shear waves propagating in the [100] and [001] directions are polarized along the [001] and [100] directions (corresponding to c_{55}), respectively (Fig. 4). Directions of maximum and minimum wave velocities remain unchanged throughout the pressure regime studied so does the direction of maximum velocity difference in shear waves due to polarization ([001])

DISCUSSION

By extending the calculations to pressures beyond 150 GPa for corundum, we find that the elastic constant c_{66}, which is equal to $(c_{11}-c_{12})/2$, increases much more slowly than c_{44} and ultimately starts to soften beyond 250 GPa. Similarly, c_{44} is shown to decrease with pressure after 400 GPa. PIB calculations (Cohen 1987) predicted this softening to occur at much lower pressures (120 GPa). In the Rh_2O_3 (II) phase c_{55} decreases at pressures higher than 150 GPa, and remains considerably smaller than c_{44} and c_{66}. The value of c_{55} is found to be highly sensitive to relaxation of ionic positions in strained lattice. In this case, macroscopic strains are likely to couple strongly with internal parameters, as in the onset of martensic transformations.

Our calculated athermal wave velocities (Fig. 5) are found to increase relatively more slowly with pressure than those derived at 300 K from sideband fluorescence spectroscopy (Zhang and Chopelas 1994). Al_2O_3 is generally expected to exist in small
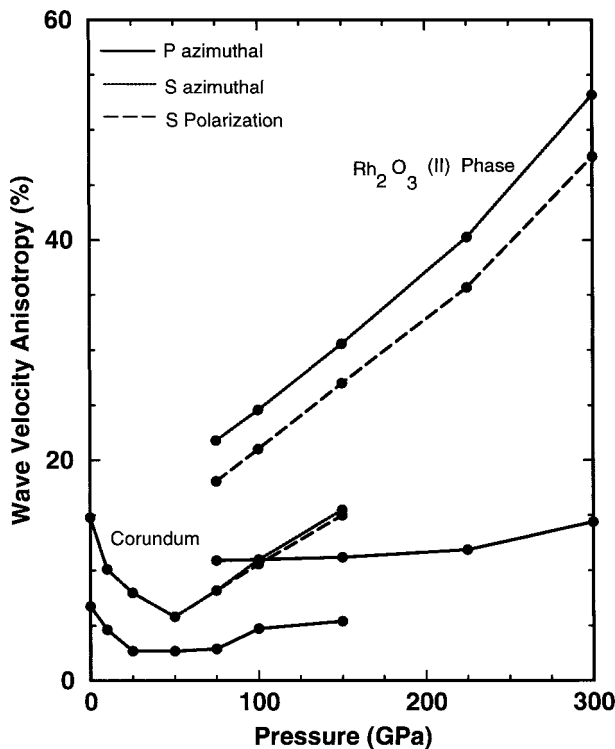

FIGURE 3. Pressure dependence of azimuthal P-wave anisotropy, and azimuthal and polarization S-wave anisotropy of Al_2O_3.

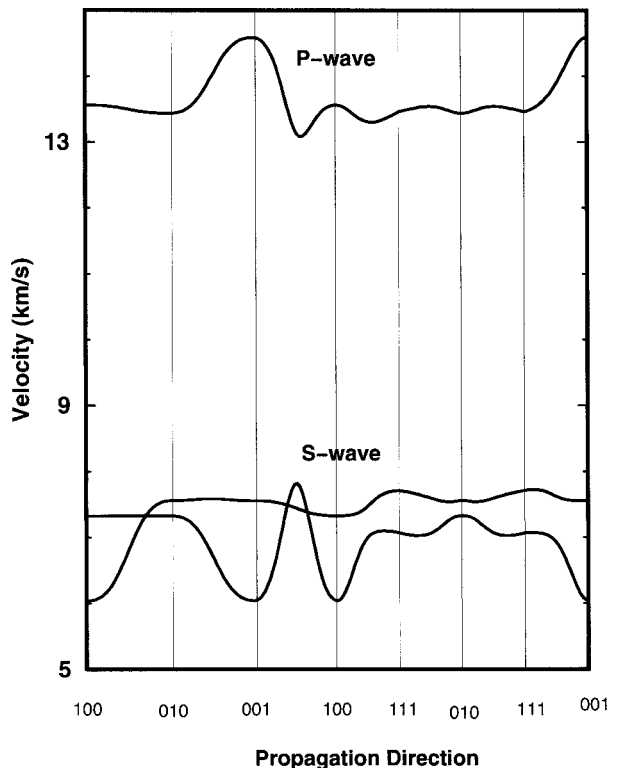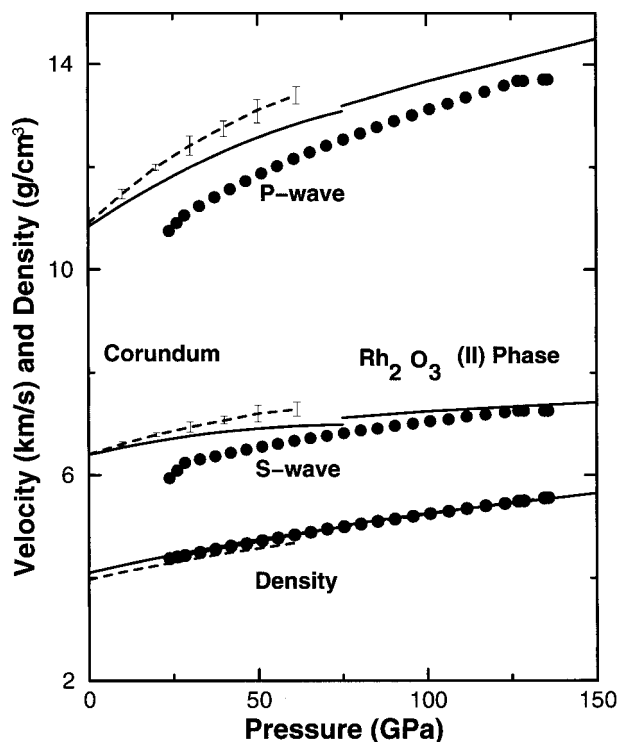**FIGURE 4.** Dependence of P- and S-wave velocities of Rh_2O_3 (II) phase on propagation direction at 100 GPa.

FIGURE 5. Density and isotropic P- and S-wave velocities of Al_2O_3 as function of pressure. The calculated properties (solid lines) are compared with the results (dashed lines) from sideband spectra (Zhang and Chopelas 1994) or from compressional data on density (Richet et al. 1988) and with the PREM model (circles) of seismic data from the lower mantle (Deziwonski and Anderson 1981).

amounts (3.6% in mass) in the Earth's lower mantle as a result of the phase transition in pyrope-garnet [$(Ca,Mg,Fe)_3Al_2Si_3O_{12}$], the most abundant Al-bearing mineral in the upper mantle, at depth of 660 km (Anderson 1989; Brown and Musset 1993). Serghiou et al. (1998) have recently shown that free Al_2O_3 from pyrope is likely to be present at pressures below 43 GPa whereas it may be accommodated in $MgSiO_3$ perovskite above 43 GPa. It is useful to compare the high pressure properties of alumina with radial variations of seismic properties of the lower mantle (Dziewonski and Anderson 1981) to understand the effect of possible Al-bearing phases on the lower mantle properties (Fig. 5). The high pressure (athermal) density is similar to the lower mantle density whereas the wave velocities are somewhat larger (about 5%) than the seismic data. The density and velocities are expected to decrease by several percents at lower mantle temperatures. Moreover, the discontinuities in density and velocities associated with structural transformation (at 78 GPa) from corundum to Rh_2O_3 (II) phase are rather small (within 2%), as shown in Figure 5. This suggests that it might be difficult to detect the presence of free Al_2O_3 in small amounts in the lower mantle through these quantities.

The D" region, i.e., the bottom 200–300 km of the lower mantle, may be enriched in the refractories such as Al_2O_3 (Anderson 1989). Because the elastic properties of alumina are comparable to the seismic observations, appreciable amounts of it may be accommodated in D". Any free alumina in this region would be in the Rh_2O_3 (II) phase, which displays substantial elastic anisotropy (about 30% polarization and azimuthal anisotropy in S waves) at these pressure conditions (Fig. 3). The D" layer is observed to exhibit significant spatially variable seismic anisotropy (Garnero and Lay 1997; Karato 1998; Lay et al. 1998). In some regions, a vertically polarized shear wave (SV) is found to be faster than a horizontally polarized shear wave (SH), whereas in other regions the opposite trend is reported. A recent first principles analysis of the anisotropy of $MgSiO_3$-perovskite, the most abundant constituent of the lower mantle, suggested that lattice preferred orientation (LPO) of $MgSiO_3$-perovskite alone may not be sufficient to explain the seismic anisotropy of the D" region (Wentzcovitch et al. 1998). Contributions from other anisotropic minerals, such as MgO, or effects of shape preferred orientation (SPO) may be necessary to explain observations. The magnitude of the transverse shear wave anisotropy of alumina ([100] aligned parallel to the vertical axis) is about 15% (SH > SV) at pressures corresponding to the base of the mantle. A weaker transverse anisotropy of about 8% (SH > SV) is obtained when [001] aligns with the vertical axis. When the alignment is along [010], the anisotropy reverses (SV > SH) and is about 10%. Therefore, on the basis of these calculated anisotropies, it is possible that lattice preferred orientation in free alumina might be contributing to the seismic anisotropy observed in the D" region, if free alumina would exist in this region.

REFERENCES CITED

Anderson, D.L. (1989) Theory of the Earth, Blackwell Scientific, Cambridge, Massachusetts.
Brown, G.C. and Musset, A.E. (1993) The Inaccessible Earth, Second Edition. Chapman and Hall, London.
Cohen, R.E. (1987) Calculation of elasticity and high pressure instabilities in corundum and stishovite with the potential induced breathing model. Geophysical Research Letters, 14, 37–40.
Cynn, H., Isaak, D.G., Cohen, R.E., Nicol, M.F., and Anderson, O.L. (1990) A high-pressure phase transition of corundum predicted by the potential induced breathing model. American Mineralogist, 75, 439–442.
Duan, W., Wentzcovitch, R.M., and Thomson, K.T. (1998) First-principles study of high-pressure alumina polymorphs. Physical Review B, 57, 10363–10369
Dziewonski, A.M. and Anderson, O.L. (1981) Preliminary reference earth model. Physics of Earth and Planetary Interiors, 25, 297–356.
Finger, L.W. and Hazen, R.M. (1978) Crystal structure and compression of ruby up to 46 kbar. Journal of Applied Physics, 49, 5823–5826.
Funamori, N. and Jeanloz, R. (1997) High pressure transformation in Al_2O_3. Science, 278, 1109–1112.
Garnero, E.J. and Lay, T. (1997) Lateral variations in lowermost mantle shear wave anisotropy beneath the north pacific and Alaska. Journal of Geophysical Research, 102, 8121–8135
Gieske, J.H. and Barsch, G.R. (1968) Pressure dependence of the elastic constants of single crystalline aluminum oxide. Physica Status Solidi, 29, 121–131.
Goto, T., Anderson, O.L, Ohno, I., and Yamamoto, S. (1989) Elastic constants of corundum up to 1825 K. Journal of Geophysical Research, 94, 7588–7602.
Hill, R. (1952) The elastic behavior of a crystalline aggregate. Proceedings Physical Society London, 65A, 349–354.
Jephcoat, A.P, Hemley, R.J., Mao, H.K., and Goettel, K.A. (1988) X-ray diffraction of ruby ($Al_2O_3:Cr^{3+}$) to 175 GPa. Physica B, 150, 115–121.
Karato, S. (1998) Seismic anisotropy in the deep mantle, boundary layers and the geometry of mantle convection, Pure and Applied Geophysics, 151, 565–587.

Karki, B.B., Stixrude, L., Clark, S.J., Warren, M.C., Ackland, G.J., and Crain, J. (1997) Structure and elasticity of MgO at high pressure. American Mineralogist, 82, 52–61.

Lay, T., Williams, Q., and Garnero, E.J. (1998) The core-mantle boundary layer and deep earth dynamics. Nature, 392, 461–468.

Marton, F.C. and Cohen, R.E. (1994) Prediction of a high-pressure phase transition in Al_2O_3. American Mineralogist, 79, 789–792.

Musgrave, M.J.P. (1970) Crystal Acoustics, 288 p. Holden-Day, San Francisco.

Richet, P., Xu, J.A., and Mao, H.K. (1988) Quasi-hydrostatic compression of ruby to 500 kbar. Physics and Chemistry of Minerals, 16, 207–211.

Serghiou, G., Zerr, A., and Chopelas, R.B. (1998) The transition of pyrope to perovskite. Physics and Chemistry of Minerals, 25, 193–196.

Shannon, R.D. and Prewitt, C.T (1978) Synthesis and structure of a new high-pressure form of Rh_2O_3. Journal of Solid State Chemistry, 2, 134–136.

Thomson, K.T., Wentzcovitch, R.M., and Bukowinski, M.S.T. (1996) Polymorphs of alumina predicted by first-principles: Putting pressure on the ruby pressure scale. Science 274, 1880–1882.

Troullier, N. and Martins, J.L. (1991) Efficient pseudopotentials for plane-wave calculations. Physical Review B, 43, 1993–2003.

Wentzcovitch, R.M., Martins, J.L., and Price, G.D. (1993) Ab initio molecular dynamics with variable cell shape: application to $MgSiO_3$ perovskite. Physical Review Letters, 70, 3947–3950.

Wentzcovitch, R.M., Ross, N., and Price, G.D. (1995) Ab initio study of $MgSiO_3$ and $CaSiO_3$ perovskite under low mantle pressure. Physics of Earth and Planetary Interiors, 90, 101–112.

Wentzcovitch, R.M., Karki, B.B, Karato, S., and Da Silva, C.R.S. (1998) High pressure elastic anisotropy of $MgSiO_3$ perovskite and geophysical implications. Earth and Planetary Science Letters, 164, 371–378.

Zhang, L. and Chopelas A. (1994) Sound velocity of Al_2O_3 to 616 kbar. Physics of Earth and Planetary Interiors, 87, 77–83.

ERRATUM

Ferrotitanowodginite, $Fe^{2+}TiTa_2O_8$, a new mineral of the wodginite group from the San Elías pegmatite, San Luis, Argentina, by Miguel Angel Galliski, Petr Černý, María Florencia Márquez-Zavalía, and Ron Chapman (v. 84, no. 5–6, 773–777, 1999).

Gene Foord contributed to our understand of the wodginite-ixiolite mineral family. "Ionilite" was a typographical error made by the editorial office.